Tellus (2008), 60A, 178–188
Printed in Singapore. All rights reserved

TELLUS

Ice dynamics in the Bothnian Bay inferred from ADCP measurements

By GÖRAN BJÖRK[1]*, CHRISTIAN NOHR[1], BO G. GUSTAFSSON[1] and AMUND E. B. LINDBERG[2], [1]*Department of Oceanography, Earth Science Center, Göteborg University, Box 460, SE 405 30, Göteborg, Sweden;* [2]*Umeå University, Umeå Marine Science Centre, Sweden*

(Manuscript received 9 February 2007; in final form 28 September 2007)

ABSTRACT

A bottom mounted ADCP has monitored the ice motion and thickness in Bothnian Bay, Baltic Sea during the entire winter season 2004. The ADCP was deployed at 20 m depth at Falkensgrund well outside the land fast ice zone. The data shows that the ice motion is primarily driven by the wind but with a clear influence of internal ice stresses. The ice stresses become more dominant as the ice grow thicker with increasing number of observations with nearly stationary ice for relatively high wind speeds. A clear dependence of the ice/wind speed ratio to wind shifts is detected with higher ratio in the new wind direction. The effect of strain hardening is also seen in several events as decreasing ice speed, sometimes to zero, in spite of constant wind speed and wind direction. A rough force balance computation gives a compressive ice strength of about 9×10^4 N m^{-2}, which is much larger than normally used in numerical ice models. The ice thickness data show numerous ice ridges with ice draft well above 1 m passing the instrument. The ridges make up a large portion, 30–50%, of the total ice volume showing that dynamical processes are important for the total ice production in the Bothnian Bay.

1. Introduction

In this study, we present and analyse observational data of sea ice drift, currents and ice thickness from a full ice season in the central part of the Bothnian Bay (Fig. 1). The observations were made with a bottom mounted Acoustic Doppler Current Profiler (ADCP) during the winter 2003–2004.

The drift of sea ice is mainly controlled by a balance between drag forces by the atmosphere and ocean, and internal stresses acting in-between ice floes and between ice floes and solid boundaries. When the internal stress is weak the coriolis force balances drag forces, and the ice motion is directed to the right of the wind on the northern hemisphere. The relation between internal stress in a medium, its material properties and the state of deformation is described by the rheology. The rheology problem of drift ice is particularly complicated since qualitatively and quantitative different laws apply to different packing densities and thickness of the ice floes (Leppäranta, 1998). One particularly important rheology parameter is the ice strength, which is primary a function of the ice thickness distribution and the compactness of the ice cover (Thorndike et al., 1975). Ice dynamics controls the deformation of the ice cover which in turn generates pressure ridges and open water. The dynamic processes are therefore intimately connected to the ice thickness distribution. For confined ice covers such in the Bay of Bothnia much of the dynamics is controlled by the solid boundaries at the coast line or land fast ice such that pressure ridges tend to build up at the windward side of the basin and open water forms at the leeward side. Better knowledge of ice dynamics and the thickness distribution has been identified as one of the key areas where more research is needed in the Baltic Sea (Omstedt et al., 2004).

The main objective with the present study is to investigate how the ice motion responds to wind forcing from different directions and how the response changes due to variations in thickness and compactness over the ice season. Earlier investigations of ice drift in the Baltic have been based on surface drifters and SAR satellite data during relatively short periods (Leppäranta, 1998; Uotila, 2001). Another aim is to obtain an estimate of the ice thickness distribution with focus on the amount of very thick ice in the form of pressure ridges. Sampling the ice thickness from a fixed position may give observations representing a long horizontal distance when the ice cover is moving. Ice motion in combination with thickness measurements from the ADCP gives a quantitative measure of the ice thickness distribution including the ridges. The abundance and thickness of ridges are important

*Corresponding author.
e-mail: gobj@oce.gu.se
DOI: 10.1111/j.1600-0870.2007.00282.x

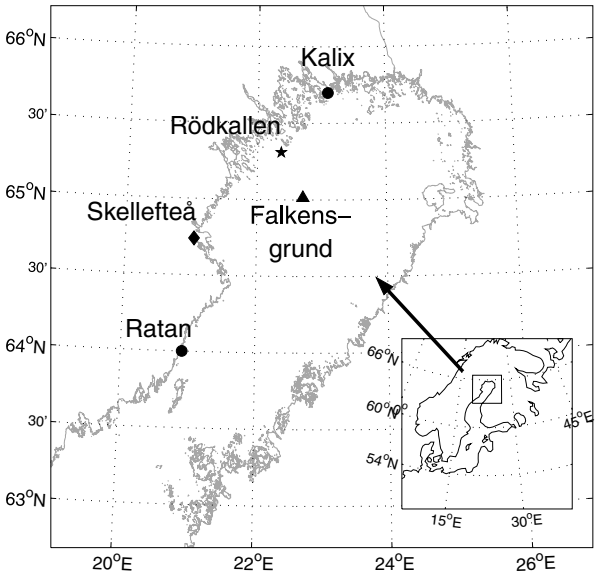

Fig. 1. Map of the Bothnian Bay with positions for the ADCP observations at Falkensgrund (triangle), meteorological observations at Rödkallen (star) and sea level observations at Ratan and Kalix (dots).

quantities for navigational purposes and ridges may also make up a large fraction of the total ice volume. Ridge formation implies a concurrent opening of the ice cover, which can increase total ice production in the basin substantially compared to thermodynamic growth of level ice. Ridges induce form drag that increases the ice water stress significantly and generate turbulence well below the water surface that may increase the overall mixing in the upper water mass. Existing data of sea ice thickness distribution from the Bothnian Bay have been relatively sparse (Jacob and Omstedt, 2005) but resent observations in 2003–2005 using an airborne Electro-Magnetic (EM) sensor has increased the amount of data significantly (EU project IRIS, 2003).

Ice charts where ice types are localized and categorized, including level ice thickness, are published regularly from the Baltic Sea and Bothnian Bay (see e.g. Swedish Meteorological and Hydrological Institute SMHI, www.smhi.se). These charts are based on satellite and mercantile vessel observations and gives therefore limited quantitative information of ice ridges (see Figs. 8–10 for examples).

The Bothnian Bay is the northernmost basin of the Baltic Sea, see map in Fig. 1. The length of the basin is 315 km, the maximal width is 180 km, and the surface area is about 36 500 km^2. The maximum depth is 120 m with a mean depth of 43 m. There is a permanent halocline at about 40 m depth, but the haline stratification is rather weak. The tides are negligibly small in Bothnian Bay due to the narrow straits towards the ocean, but sea level variations due to other processes (mainly wind forcing and air pressure variations) can be quite large with typical amplitudes in the range 0.3–0.5 m (Samuelsson and Stigebrandt, 1996) (see also Fig. 3).

Winters are severe enough to cause sea ice formation in the Bothnian Bay every year. Mean ice thickness varies depending of the severity of the winter, but typically level ice becomes 50–120 cm thick (Leppäranta and Omstedt, 1999). Ice formation generally starts in the shallow coastal areas in the north and thereafter it spreads into the inner parts. Fast ice is usually found landward of the 10 m isobath (see Granskog et al., 2006 for a review of Baltic Sea ice properties). The Bothnian Bay is large enough for the wind forcing to overcome the ice strength and the ice cover deforms therefore during strong wind events and pressure ridges are formed (Leppäranta, 1981; Uotila, 2001). Pressure ridges are typically 5–15 m to a maximum of about 30 m (Leppäranta and Hakala, 1992). The wind is generally rather uniform over the basin since it's size is relatively small compared to the typical scale of atmospheric low pressure systems. Hence, pressure ridges are primarily formed on the windward side of the basin and leads are formed at the upwind side. Thin young ice is formed rapidly in the leads during cold winter conditions.

2. Observations and data processing

An upward looking ADCP was deployed on the sea floor at 21 m depth on the Falkensgrund (N 65°00.80′, E 22°42.48′, see map in Fig. 1). The deployment site was selected in order to be shallow enough to give a distinct echo from the ice but deep enough to avoid the keels of passing ice ridges. The large distance to the shore kept the instrument well outside the fast ice zone.

The instrument, a RDI 600 kHz ADCP, stored ensembles of measurements every 10 min, each consisting of 160 water track pings and 40 bottom track pings. The beam angle is 30° and the beam width for each beam is 3° giving a footprint with a diameter of about 1.2 m for each beam and total footprint area of about 23 m including all beams. A 1 m vertical bin size was used, resulting in an error standard deviation of 1.8 cm s^{-1} for the water velocity. The bottom track measurement was used to detect ice velocity and has an error standard deviation of about 1 cm s^{-1}. The zero velocity offset is typically 0.5 cm s^{-1} for this type of instrument.

Wind and air temperature observations are from the meteorological station Rödkallen, see Fig. 1). The atmospheric data are given every 3 h and were interpolated in time to fit the ADCP data set.

The ice draft can be estimated using the distance between the ADCP and the depth cell with maximum echo intensity. The bin size of the ADCP is 1 m, but it is possible to increase the resolution to about 0.1 m by fitting a modified Gaussian curve to the vertical echo intensity distribution (Shcherbina et al., 2004). The maximum point of the Gaussian curve was then used to determine the distance from the instrument to the lower ice surface. This method was applied on the echo intensity distribution for each of the four beams giving four time-series of distance data. These time-series was then transformed using empirical

orthogonal functions EOF in order to quantify the covariance between the four beams. The time-series of the first orthogonal mode was finally used as a measure of the distance from the instrument to the lower ice surface.

This distance is not only dependent on the ice draft but also on the sea level. The actual ice draft was determined by subtracting the observed sea level. Sea level observations from coastal mareograph stations at Ratan and Kalix where used (see Fig. 1). The average of these two stations was used to represent the sea level at Falkensgrund. The sea level measurement frequency is 1 h and these data were also interpolated to fit the ADCP data set.

It turned out to be quite straightforward to determine whether there is open water or ice above the instrument since open water results in enhanced variance of the error velocity, which is a measure of the difference in vertical velocity between the four beams. Wave motions in open water gives different vertical motion for each beam and therefore large error velocity. In the present data set it was found that open water increases the variance of the error velocity with a factor 3. Similar results was obtained in a study using ADCP from the Gulf of St. Lawrence (Belliveau et al., 1990).

3. Results

The first ice was observed at Falkensgrund on January 16, 2004. Thereafter a persistent ice cover was observed until the ice broke up at May 8, except for a brief period between Jan. 24–28. The three full calendar months (February–April) with ice observations is used in the subsequent analysis.

Time-series of air temperature, wind, ice velocity and water velocity are shown in Fig. 2. The temperature was generally well below zero until mid-April, when it became less variable and systematically above 0°C. The winds were generally moderate with just a few occasions with speed above 10 m s^{-1} and there was a clear correlation between southerly winds and high air temperature and vice versa. Significant ice movements occurred in events with high velocities correlated with strong wind velocities and nearly motionless periods in-between. The maximum ice speed recorded was about 50 cm s^{-1}. Currents 2 m below the ice had generally similar direction as the ice motion, but current speeds were lower indicating that the dominating forcing on the ice cover came from the atmosphere rather than from the sea, as will be discussed further below.

3.1. Ice thickness distribution

The time-series of ice draft computed from echo intensity and adjusted for sea level variations is shown in Fig. 3a and sea level variations at Ratan and Kalix in Fig. 3b. Ice draft of more than 1 m occurred frequently representing pressure ridges passing over the instrument. The maximum draft obtained by this method is about 7 m. It should be noted that the amount of thick ice is artificially exaggerated in this plot since many peaks are merged together by the relatively coarse plot resolution. Figure 3c gives an example with much higher temporal resolution of the echo intensity, ice velocity and the estimated ice draft during a 4-d period. This period started with near zero ice motion (red curve) and nearly constant ice thickness (seen as a very regular and distinct maximum of the echo intensity). The ice started to move on the evening March 26 and numerous ridge-like structures passed the instrument during the late evening and the following day. These appear as a downward displacement of the maximum echo intensity, which is used to determine the ice draft. The ice draft is shown by the white curve.

Although the echo intensity shows a very clear signature of pressure ridges, this method to obtain ice draft is not without problems. The main difficulty is that the echo intensity data are

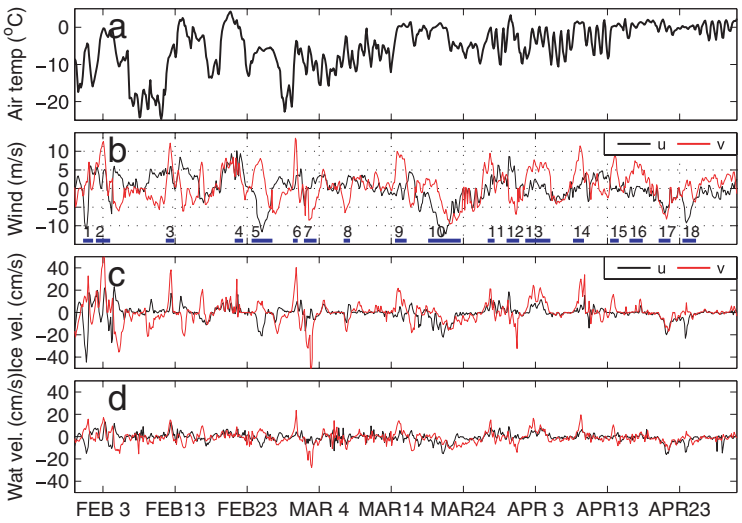

Fig. 2. Overview of the meteorological observations and ADCP measurements during the ice season 2004. (a) Air temperature at Rödkallen. (b) Wind speed components at Rödkallen in geophysical coordinates (u is positive eastward, v is positive northward). The same coordinates are used in the (c) and (d) panels. The thick blue line segments indicates events with wind speed above 5 m s^{-1} that are analysed separately in Figs. 5, 8, 9 and 10. (c) Ice velocity components from Falkensgrund (3 h means) based on bottom track data from the ADCP. (d) Water velocity components (3 h means) at a distance approximately 2 m below the ice based on ADCP data from the water column.

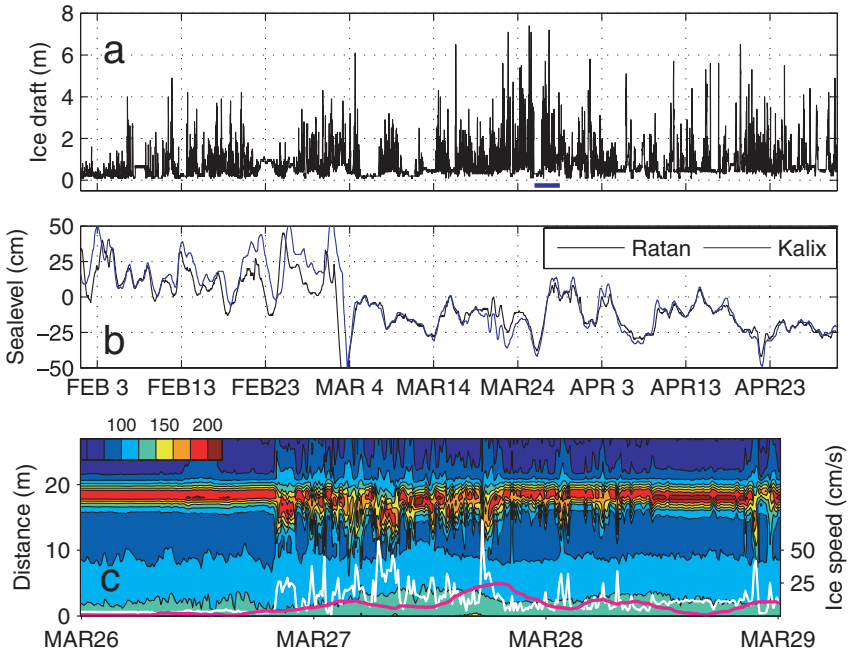

Fig. 3. (a) Ice draft based on ADCP data. The distance from the instrument to the bottom ice surface is determined by fitting a Gaussian curve around the ADCP grid cells containing the maximum echo intensity (see also panel c and method section). The ice draft is then determined by subtracting this distance from the total distance to the sea surface (including sea level variations). The sea level at the observation site is defined as the mean value between the sea level observations at Ratan and Kalix. (b) Sea level observations at Ratan and Kalix. (c) Magnification of a short period (indicated by the thick line segment in panel a) of the ADCP observations. The colour contours show echo intensity as a function of vertical distance from the instrument in decibels (the colour scale is shown in the upper left corner). Also shown is 2× ice draft (white curve) referred to the left *y*-axis, and the ice speed (thick red curve) referred to the right *y*-axis.

averaged over a sampling interval of 10 min. The actual ice draft can vary considerably during the sampling interval and small scale structures during periods with high ice speed are not resolved. An ice speed of 20 cm s^{-1}, for example, corresponds to a measurement cell with a length of 120 m. It can be assumed that many pressure ridges have a smaller horizontal length scale, and such ridges will therefore not be sampled properly. A pressure ridge of smaller scale than the measurement cell will still be seen in the average echo intensity as enhanced values over a number of depth cells (instrument bins) below the level ice surface, where the number of affected cells depends on the ridge thickness. It is however not certain that the position of the maximum echo intensity is affected to the same degree. It is likely that the average maximum echo intensity will be at nearly the same position as for the level ice. Using the maximum echo intensity will therefore sometimes underestimate the ice draft. Another potential problem with the present method is that it might be large differences of the ice draft obtained from the individual beams. This can make it difficult to determine a true draft based on all beams. The first empirical mode based on draft data from the four beams explains however about 87% of the total variance. This shows that individual beam data covaries to a high degree and occasions with large draft differences between beams are rare. The deviation of sea level between the stations is at most about 20 cm as seen in Fig. 3b. The deviation is much less during most of the time and we estimate that the typical error in sea level at Falkensgrund is less than 10 cm.

When observing the ice thickness distribution at a fixed point there is a risk of measuring the same portion of the ice cover passing back and forth above the instrument. That would result in an observed ice thickness distribution that is not representative for a larger area. However, in the Bothnian Bay where the ice seems to move in long trajectories, typically 10–30 km (see Fig. 5), the probability is very low that the same portion of the ice cover will return to the observation point.

The ice thickness distribution is computed using the ice thickness weighted by the length of the measurement cell for each ensemble. The length of the measurement cell is ice speed (3 h moving average) multiplied with the sampling interval (10 min). The ice thickness distribution for each month and for the entire period is shown in Fig. 4. We judge it not relevant to have a finer resolution than 1 m in the thickness increment since the ice thickness obtained by the present method is relatively uncertain. We expect that the error is less than ±0.3 m for level ice but as noted above the error can be larger, and systematically underestimate the ice draft for thick structures with small horizontal scale and passing at high speed.

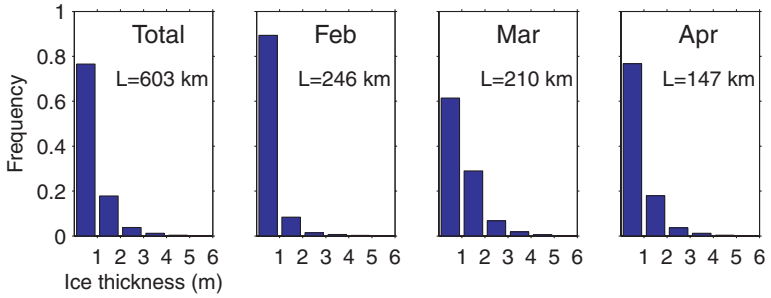

Fig. 4. Total thickness based on ice draft distribution for the entire period (February–April) and distribution for each month. The observations are weighted by the length of each measurement cell defined as the ice speed (3 h moving average) multiplied with the sampling interval (10 min). The distribution is normalized by the total observed track length, L, for each period. L is the sum of the length of the measurement cells.

Table 1. Ice thickness based on ice draft statistics for different months and for the entire period based on ADCP echo intensity data. The mean ice thickness Hm is defined as $Hm = \frac{1}{L}\sum_{i=1}^{n} d_i H_i$, where H_i is the ice thickness for each observation and d_i is the length of each measurement cell, defined as the observed ice speed (3 h mean) multiplied with the sampling interval (10 min). L is the total length of the observation track $L = \sum_{i=1}^{n} d_i$. The volume fraction of ridges VR is defined as $VR = \frac{1}{LHm}\sum_{i=1}^{n} d_i H_i (H_i > 1m)$

	February	March	April	Total
Hm (Mean ice thickness) (m)	0.43	0.99	0.77	0.73
VR (Ridge volume fraction)	0.32	0.61	0.45	0.49

Most of the ice was thinner than 1 m, as expected in this area where the level ice rarely becomes thicker than 1 m. The thinnest fraction occupied about 90% in February, 60% in March and 78% in April. Ice thicker than 1 m represents pressure ridges and there were thus 10% of ridges in February, 40% in March and 22% in April (see also Table 1). The ridges constituted a large proportion of the total ice volume as seen in the table. The results suggest that between 30 and 60% of the ice volume in the central Bothnian Bay consists of ridges at least during this particular ice season. This data set represents a total observed track with a length of 600 km which is about two to three times the size of the basin and should thus give a fairly representative ice statistics for the central part of the bay.

3.2. *Ice dynamics*

The Bothnian Bay is large enough so the accumulated wind force across the basin can overcome the ice strength during most circumstances and the ice will move even if the basin is completely ice covered. However, during extremely cold winters with very thick level ice (>0.5 m), the ice cover may become nearly stationary (Haapala and Leppäranta, 1996). The 2004 season was rather mild so the ice cover was mobile during the entire winter.

The ice was nearly stationary for wind speeds less than about 5 m s^{-1} (Fig. 2) but there was still some motion during most of the time. The ice cover could be defined as stationary for only about 3% of the observations having a speed less than 0.5 cm s^{-1} which is the threshold of the instrument. The ice speed was small, $<$10 cm s^{-1}, for about 70% of the observations. The high speed part of the record, with speed $>$10 cm s^{-1}, was characterized by relatively well defined events with maximum speeds between 20 and 50 cm s^{-1}. These high speed events represent a major part (about 70%) of the total drifting distance of the ice (defined as the ice speed times the sampling period and summed over all observations). It is therefore relevant to analyse the direct dynamic response of the ice to wind forcing event by event. We found 18 events during the winter season with wind stronger than 5 m s^{-1}. These are indicated in Fig. 2b. Figure 5 shows progressive vector diagrams of ice and wind for these events. The wind vector has been scaled with a factor of 0.03, which is a typical ice/wind speed ratio. This ratio may actually vary between 0.02 and 0.035 depending on the ice roughness where the low value represents a deformed ice cover with frequent pressure ridges and the high value a smooth ice surface (Leppäranta, 2005). It should be noted that effect of the coriolis force on the free drift speed and turning angle is negligible for the present relatively thin ice cover having a Rossby number (coriolis force/water drag force) typically less than 0.1.

Extensive ice motion occurred in all events throughout ice season. Typical translations were 10–30 km during the events corresponding to 5–20% of the basin scale (about 150 km). Since the basin was almost completely ice covered during the entire winter each event must have caused substantial ice deformation and ridge building.

Event 1 was the only one with free drifting ice, i.e., without any significant internal ice stresses or influence of water motions. The ice and wind trajectories have nearly the same length and the ice moved at an angle to the right of the wind vector. The trajectories are also of similar length in event 2, but the ice moved to the left of the wind vector. During this event, the ice motion was significantly affected by a strong barotropic oscillation in the ocean with an amplitude of about 20 cm s^{-1}. The oscillation is barely seen in Fig. 2 but is a dominant feature in the entire water column data. Internal ice stresses dominated later on during the season causing ice trajectories to be shorter than free drift scaled wind trajectories. There was one event at the end of the ice season (in April, event 16) when the ice moved only

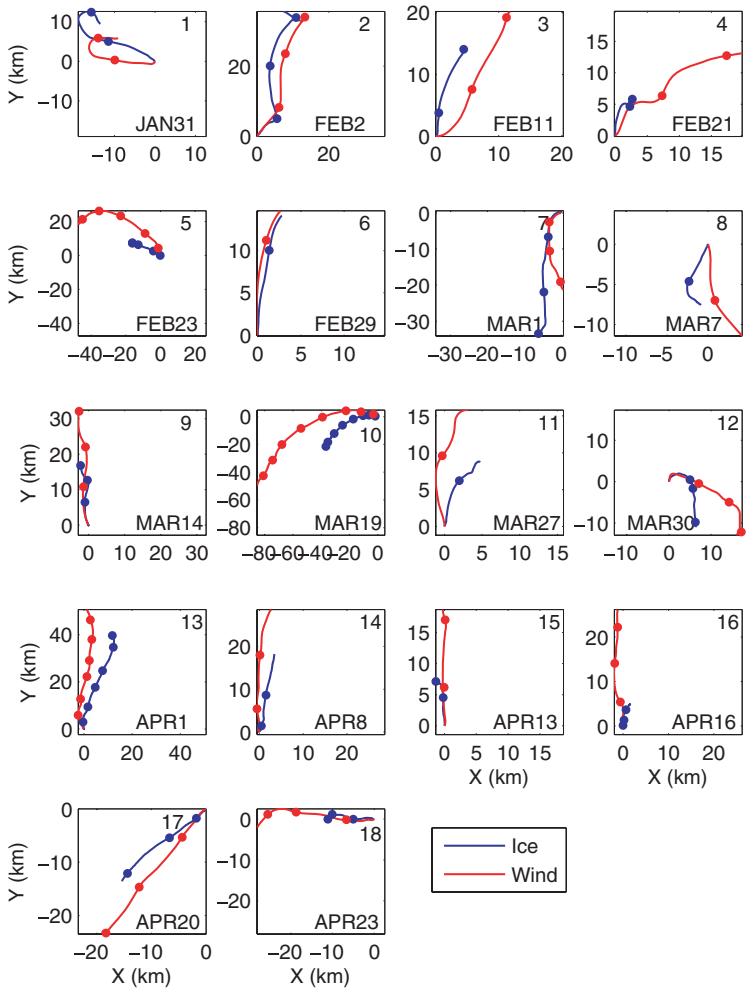

Fig. 5. Wind and ice trajectories for events with wind speed larger than 5 m s^{-1} (see Fig. 2 for time period of each event). The wind components has been multiplied by a factor 0.03 so that equal length of the trajectories would roughly represent free drift. Event number (top) and start date (bottom) for each event are also shown. The elapsed time along each trajectory is roughly indicated by a dot every 12 h.

about 5 km compared to about 25 km for free drift. This event was the last of four events with southerly winds that packed the ice towards the northern part of the bay and thereby enhanced the strength against deformation. There is a general tendency that the ice is more mobile in events characterized by a large directional shift of the wind compared to the previous event. This is especially clear when comparing event 16 and 17. When the northeasterly wind started in April 20, it occurred after a long period of southerly wind and the ice moved easily in the new (reversed) wind direction. Ice charts (not shown) confirmed that the period of southerly winds formed a large open area in the southeastern part of the bay, which made it easy for the ice to move in that direction.

An overview of how the ice speed responds to wind forcing can be obtained from a two-dimensional frequency plot of wind and ice speed. Such plots are shown in Fig. 6 for each month and are based on 3-h mean ice and wind speeds. For an ice cover in free drift all data would be concentrated along a line with a slope related to the ice/wind speed ratio (a line with 3% slope is indicated in the figures). This is not the case for the observations from Bothnian Bay where the data is very much spread over the wind/ice speed plane. There is a weak tendency to a concentration of data around the free drift line in February but most of the observations fall below the free drift line indicating a large influence of internal stresses. There are also some observations with faster ice motion than 3% of the wind speed, probably due to influence of ocean currents acting in the wind direction. The ice speed was generally reduced in March with few observations higher than 25 cm s^{-1} and a larger dominance of data points below the free drift line. The was also significantly more observations with ice speed less than 5 cm s^{-1}. The winds were generally weaker in April with just two occasions above 10 m s^{-1}, but there is still a clear tendency that the ice cover was much less mobile than earlier in the season with many more observations with ice speed below 5 cm s^{-1}. There were, for example, 110 occasions (corresponding to about 14 d) in the wind speed range 2–5 m s^{-1} having ice speed less than 5 cm s^{-1}. The ice cover was thus nearly stationary for low wind speeds. It should also be noticed that even though the ice cover was nearly stationary for most of the time, there were still events when it

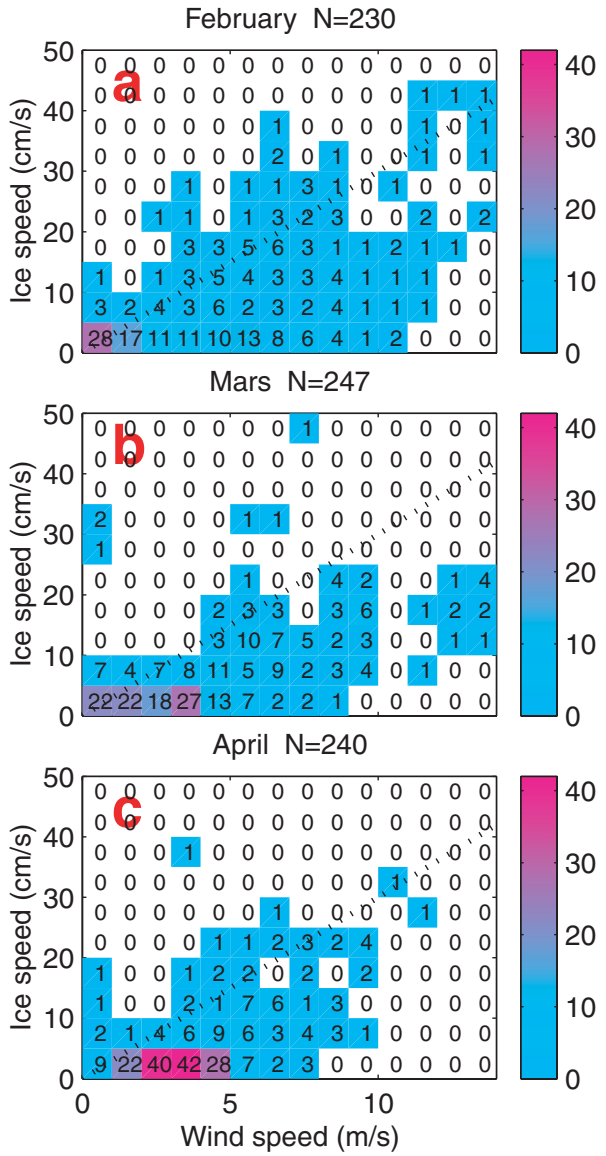

Fig. 6. Two-dimensional frequency plot of wind and ice speed for each month based on 3 h mean ice speeds. (a) February, (b) March and (c) April. The wind and ice speed is divided into 1 m s^{-1} and 5 cm s^{-1} bins, respectively. The dotted line indicates roughly the free drift relation when the ice velocity is 3% of the wind speed. The number of occurrences in each bin is given both by numbers and a colour scale. The total number of occurrences (3 h means) N for each month are also given.

moved in near free drift. This is likely due to areas of thin new ice or open water that usually are formed close to the coast. The ice can easily move towards such areas if the wind direction is favourable.

The percentage of observations with nearly stationary ice cover (ice velocity <5 cm s^{-1}) for different wind speed intervals is summarized in Table 2 for each month. This gives a measure

Table 2. The percentage of observations with near zero ice motion (0–5 cm s^{-1}) for different wind speed intervals

Month	2–3 m s^{-1}	3–4 m s^{-1}	4–5 m s^{-1}	5–6 m s^{-1}	6–7 m s^{-1}
February	64	50	42	50	30
March	72	77	45	26	9
April	90	80	68	30	14

of how the stiffness of the ice cover (resistance to move with the wind) developed over the season. The percentage of observations with nearly stationary ice cover increased over the season for all three wind speed intervals up to 5 m s^{-1}. The ice was, for example, nearly stationary in 50% of the observations in February in the wind speed interval 3–4 m s^{-1} but in April this occurred for 80% of the cases. However, the ice still moved rather easily for wind speeds above 5 m s^{-1} even in April. The ice speed is then larger than 5 cm s^{-1} in 70% of the observations.

A more objective way to examine the relation between wind forcing and ice motion is to assume a linear dependence between the wind and ice velocity by fitting a linear regression model to the data. The ice/wind relationship is given by: (1).

$$U_{\text{ice}}(t) = R(t)U_{\text{wind}}(t) + Z(t), \tag{1}$$

where all involved quantities are complex numbers. $R(t)$ is the temporally varying complex regression coefficient involving a wind/ice speed ratio and a turning angle. $Z(t)$ contains the portion of the ice motions not explained by the wind forcing. $R(t)$ is computed by minimizing the least-square error between the model and observations over a time window δ_t, that is,

$$R(t) = \frac{\langle U_{\text{ice}} U^*_{\text{wind}} \rangle - \langle U_{\text{ice}} \rangle \langle U^*_{\text{wind}} \rangle}{\langle U_{\text{wind}} U^*_{\text{wind}} \rangle - \langle U_{\text{wind}} \rangle \langle U^*_{\text{wind}} \rangle}, \tag{2}$$

where means are computed as

$$\langle U \rangle = \frac{1}{\delta_t} \int_{t-\delta_t/2}^{t+\delta_t/2} U(\tau)\, \mathrm{d}\tau \tag{3}$$

and the stars denotes complex conjugates. The length of the time window is a trade-off between the possibility to detect changes in the wind/ice relation and to include enough covariability to get a significant regression. A window shorter than 5 d gives a very unstable regression coefficient with large fluctuations indicating that wind forced variability occur on longer timescales. We use a 10-d window that both gives a stable regression and a possibility to see changes in the relationship over the period. The wind/ice speed ratio plot and the associated angle for different months is shown in Fig. 7a. The speed ratio was around 3% in the beginning of February, decreased to just above 1% in the middle of the month and went back up to 3% at the end of February and early March. The ratio was relatively low, between 1–2%, during the rest of the period. The rapid decrease of the speed ratio in the first part of the period shows that ice stresses became dominant rather quickly, presumably as a result of the increasing new ice

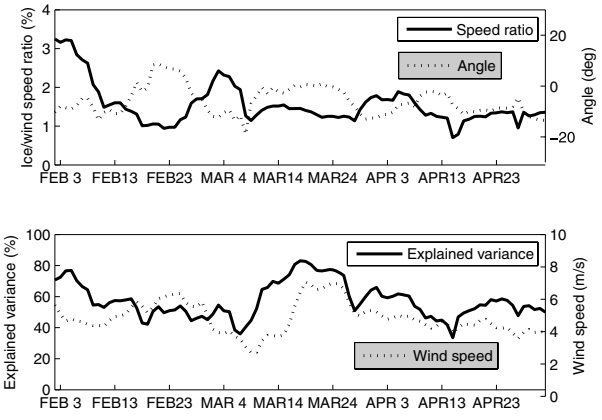

Fig. 7. (a) Ice/wind speed ratio and turning angle based on a linear regression model (eq. 1) using a 10 d time window. The time window is incremented by 1 d. (b) Explained variance and average wind speed over each 10 d window.

thickness. The enhanced speed ratio during some periods, as in late February, can be explained by shifts in the general wind direction. The event in late February was the first occasion of northerly winds after a period of mostly southerly and easterly winds (see Fig. 5) and it was then easy for the ice to move towards thinner ice in the south. There is no tendency that the ice becomes more mobile just before it disappears in early May which is somewhat unexpected because large amounts of open water are normally associated with the break-up which should increase the mobility. The break-up period was however dominated by southerly winds that hold the remaining ice cover in the northern part of the bay.

The turning angle was generally negative meaning that the ice moved to the right of the wind direction. It was about -10° at the beginning of the period, which is less than typically -30° that would be expected in free drift (Thorndike and Colony, 1982) indicating some influence of ice stresses already for the initially thin ice cover. There was also a relatively long period in the middle of the record with near zero angle, again showing the influence of the internal stress. The explained variance, that is how much of the variance of the ice motion that is explained by the linear model for each time window, was high, about 80%, in the beginning of the record and in March. Between these periods the explained variance was relatively low (40–60%) showing a less direct relation between ice and wind velocity. The explained variance is somewhat dependent on the wind speed with higher values for higher wind speeds which is natural since one should expect a clearer wind dependence for strong winds when the wind force can overcome the internal stress.

The observations can be examined in terms of force balance in order to acquire quantitative information on the partitioning between air stress, water stress and internal ice stress. We examine three characteristic events in more detail: One event in near free drift (event 1), one relatively short event with significant ice stress (event 5) and a long event dominated by ice stress (event 10).

The force balance neglecting the acceleration, coriolis and sea surface tilt terms is given by

$$\tau_\mathbf{i} + \tau_\mathbf{a} + \tau_\mathbf{w} = 0, \tag{4}$$

where $\tau_\mathbf{a}$ is the air stress, $\tau_\mathbf{w}$ water stress and $\tau_\mathbf{i}$ internal ice stress. $\tau_\mathbf{a}$ and $\tau_\mathbf{w}$ can be computed from data while $\tau_\mathbf{i}$ is given as the difference vector. The air and water stress are computed according to:

$$\tau_\mathbf{a} = \rho_a C_a |\mathbf{U_w}| \mathbf{U_w} \tag{5}$$

$$\tau_\mathbf{w} = \rho_w C_w |\mathbf{U_2} - \mathbf{U_i}| (\mathbf{U_2} - \mathbf{U_i}), \tag{6}$$

where $\mathbf{U_w}$ is the wind velocity, $\mathbf{U_i}$ ice velocity, and $\mathbf{U_2}$ water velocity 2 m below the ice. Stresses and velocities are all vector quantities. ρ_a and ρ_w are the air and water density, respectively ($\rho_a = 1.3$ kg m^{-3}, $\rho_w = 1000$ kg m^{-3}). The air drag coefficient Ca $= 1.5 \times 10^{-3}$ is based on 10 m wind speed observations from Joffre (1982). The ice/water drag coefficient C_w is estimated from the ADCP water velocity data 2 m below the ice, U_2. A value $C_w = 3.0 \times 10^{-3}$ was found to give a realistic force balance during free drift. We use a drag coefficient based on ocean velocities relatively near the ice in order to obtain a direct connection between the ice–water velocity difference and the surface stress. The 2-m distance below the ice is chosen in order to be as close as possible to the ice but still having ADCP data from the water column that is free from disturbances by the strong echo from the bottom surface of the ice (ADCP data from the depth cell closest to a strong reflector tends always to be corrupted). Another possibility is to use current velocity well below the turbulent upper boundary layer, which is usually referred to as the free geostrophic velocity. In that case one needs also to incorporate a turning angle between the geostrophic current and the surface stress. Effects of stratification needs then probably also to be taken into account.

Event 1 occurred early in the season when the ice was thin (5–20 cm according to the ice chart) and the ice cover should therefore primarily be in free drift and the force balance should be dominated by air stress and ice–water stress. Fig. 8 shows the ice speed and force balance during event 1. The chosen value of C_w gives an ice/water stress that matches the air stress relatively well over most of the period. The length of the difference vector $\boldsymbol{\tau}_\mathbf{i}$ (which can interpreted as internal ice stress) is also much smaller than the two other stresses. It should be noted that the ice/wind speed factor is well above 0.03 during a larger part of the event (Fig. 7a), which is higher than other observations during free drift conditions. Leppäranta and Omstedt (1990) report a factor 0.02 during a 7 d experiment in April. It is likely that the present event, early in the season, is characterized by relatively smooth ice surface with relatively few ridges giving a low water stress that in turn brings up the ice wind factor compared to the April observations with more ridges.

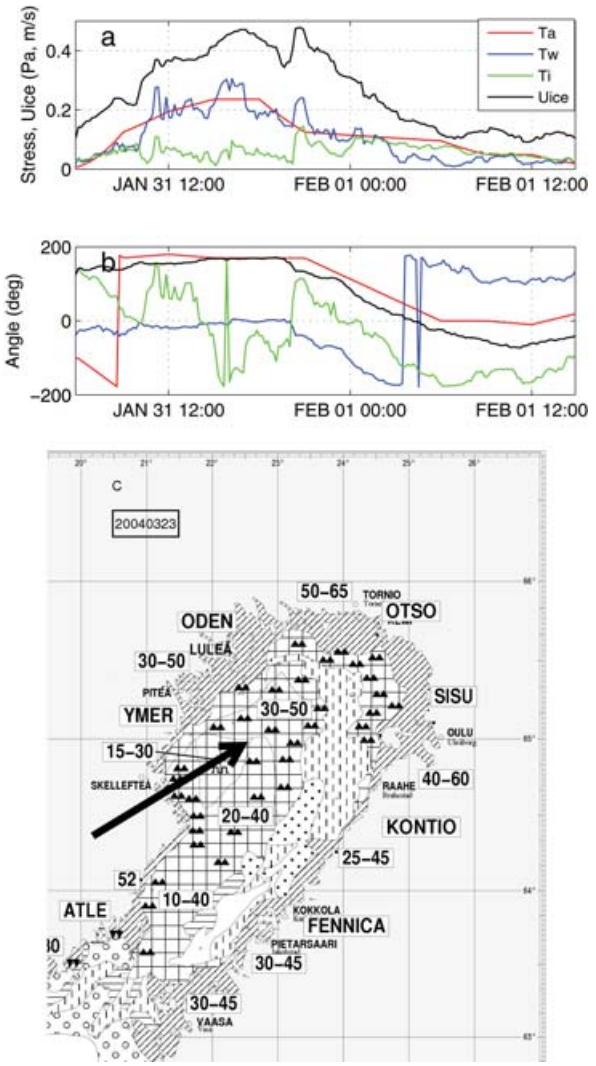

Fig. 8. Stress vectors and ice velocity vector during the period 01/31–02/01 (event 1 in Fig. 2). The (a) panel shows magnitudes and the (b) panel the angle in the geophysical coordinate system (90° represents a vector pointing in the northward direction). Ta is the air stress, Tw is the water stress, Ti is the internal stress and Uice is the ice velocity. All time-series are low-pass filtered by a 1 h moving median filter. Panel (c) shows ice chart from February 2, reproduced with permission by the Swedish Meteorological and Hydrological Institute (SMHI). The numbers within squares are ice thickness in cm and the arrow shows the position for the ADCP measurements. Symbols for ice-types are defined as: Checked pattern denotes consolidated, compact ice (9–10/10); horizontal hatching close ice (7–10/10); vertical bars open ice (4–6/10); circles very open ice (1–3/10); stars new ice; dots open water; inclined hatching fast ice; and triangles denote pressure ridges.

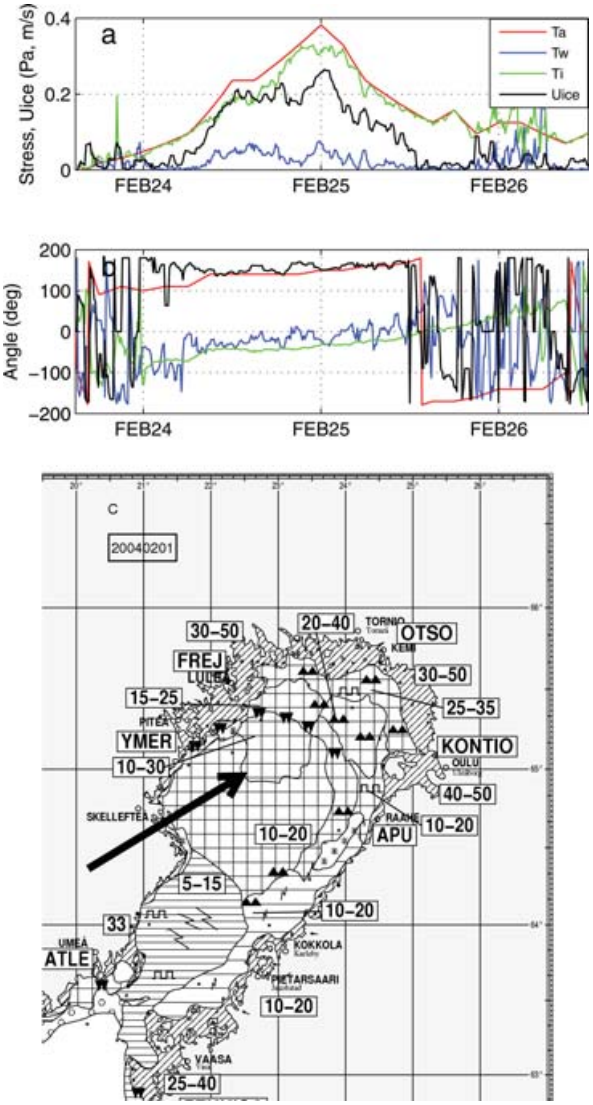

Fig. 9. Same as Fig. 8, but for the period 02/24–02/26 (event 5 in Fig. 2.)

The next event (no 5) is characterized by significant ice stresses (Fig. 9). The ice thickness according to the ice charts was 15–40 cm over a large part of the basin. The wind direction was from southeast in the beginning of the event and turned gradually towards east and northeast. The ice started to move significantly when the air stress exceeded 0.1 Pa and the speed increased until it levelled off at about 0.2 m s^{-1} in spite of continued increased air stress. $|\boldsymbol{\tau}_\mathbf{w}|$ was much smaller than $|\boldsymbol{\tau}_\mathbf{a}|$ during the event showing the dominance of internal ice stress. This is an example of strain hardening such that the internal ice force increases as the ice becomes compacted. There was a second peak in ice velocity, possibly due to the change in wind direction exposing a somewhat weaker part of the ice cover to the air stress. The ice stopped moving at around 0.15 Pa air stress while it started to move at a much lower stress level (∼0.08 Pa).

Event no 10 (Fig. 10) is an example of a longer wind event when the wind direction slowly shifted from easterly to northeasterly. The effect of successive strain hardening can be seen during this event such that the ice became stronger the more it was compacted. The ice started to move easily for air stress at about 0.1 Pa but the internal ice stress built up rapidly and

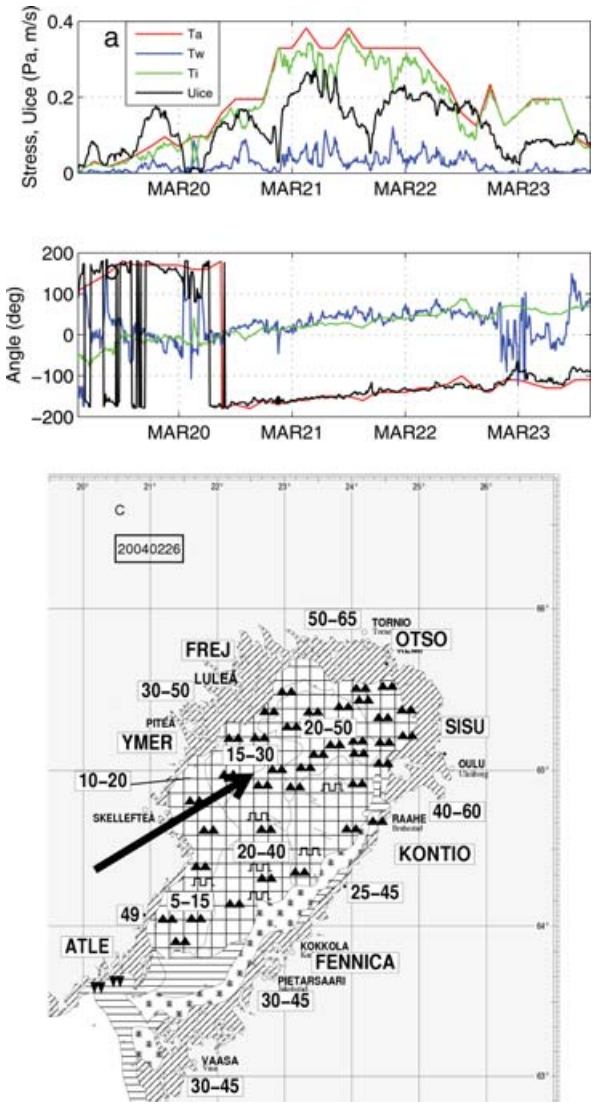

Fig. 10. Same as Fig. 8, but for the period 03/20–03/23 (event 10 in Fig. 2.)

stopped the motion. When the air stress later on increased to about 0.2 Pa it overcame the ice strength and the ice started to move, reached a maximum, and stopped again due to increased internal stress. The same pattern repeated on the third day when the air stress increased to >0.3 Pa with an associated peak in ice velocity. A second peak in the ice velocity occurred during this relatively long period of high and relatively constant air stress. This was probably due to slightly changing wind direction towards more northerly so that a weaker part of the ice cover became involved in taking up the wind load. It is possible that the peninsula southeast of Skellefteå (Fig. 1) no longer posed an obstacle when wind shifted and the ice could pass more freely in the southward direction.

It is possible to obtain a rough estimate of the compressive ice strength from the internal ice stress and the wind fetch over the basin. The maximum ice stress during event 10 with near zero velocity was about 0.3 Pa which multiplied with a fetch of about 150 km gives a force of 4.5×10^4 N m^{-1}. In order to obtain an ice strength this should be divided with an ice thickness, which is rather uncertain, but using 50 cm which was the maximum level ice thickness in the area according to the ice chart gives an ice strength of 9×10^4 N m^{-2}. This is actually much larger than the 2.5×10^4 N m^{-2} that has been used as a working standard in ice models of the Baltic (Leppäranta et al., 1998). This difference by a factor of three is somewhat surprising since 50 cm should be about the thickest level ice present in the basin during this season. If thinner ice had to take up the wind load the difference would have been even larger. Another possibility is that the ice cover was heavily ridged in the area for maximal ice stress so that the effective load up-taking thickness was larger than 50 cm. It should be mentioned that higher values of the yield strength, up to 100 kPa, have been obtained by comparing surface elevation data for open water and compact ice (Zhang and Leppäranta, 1995).

4. Discussion

The single fixed instrument in the central part of the basin provides some basic information of the dynamic response of the ice cover to wind forcing, but it gives certainly not the full picture. It is well known that the motion field varies in space it is an open question over how large area this single point measurement gives a representative measure of the ice motion. Drifter data shows, for example, that the ice motion becomes more aligned along the coastline in the shear zone close to the coast (Uotila, 2001). It would be interesting to have observations at several locations in order to quantify spatial variations of the ice motion. Spatial information can already be obtained from drifting buoy data (Uotila, 2001) and pattern following systems based on satellite pictures (Leppäranta et al., 1998). An advantage with fixed instruments below the ice is that currents and ice thickness can be measured simultaneously with ice velocity. Fixed point observations also provide high time-resolution data compared to satellite products and a better control of the observation location compared to drifting buoys which will be transported over long distances.

The ice draft derived from the ADCP is probably underestimated especially for small scale structures and high ice speeds primarily due to the 10 min long averaging period of the ADCP data. It is hard to estimate how large this error is without comparing simultaneous ADCP data with, for example, data from an upward looking sonar with much higher sampling frequency. Other investigations based on drilling Leppäranta and Hakala (1992) and EM data from the extensive IRIS field champagne on eastern Bothnian Bay 2004 show that ridges thicker than 5 m are relatively frequent. One aspect in favour of reducing the error with the present method is that structures giving an enhanced echo intensity well below the level ice surface and no associated change of the position for the maximum echo intensity are rare in the present record. The short period shown in

Fig. 3c is in fact representative for the entire observational record. This means that ridges are always detected but the maximum thickness for an individual ridge might still be underestimated. It is therefore likely that the amount of ridges ice >1 m in the obtained thickness distribution is realistic.

The present study has some implications on ice models for the Baltic and likely also for other semi-sized basins with perennial ice cover such as the Great lakes, the White Sea and the Hudson Bay. With semi-sized is meant here that the basin is large enough to have moving ice but small enough so that the atmospheric forcing is nearly uniform. A characteristic feature for the Bothnian Bay is the formation of open water and new ice at the leeward coast. The size of this area is a critical quantity to reproduce by ice models. It is important to describe the opening area correctly since it will be the place for large production of new ice and it will also represent a build-in weakness of the ice cover for winds in the opposite direction. If the size of new ice area is reasonable correct one can also expect the rheology of the ice model, including the parameters such as the ice strength, to work properly. Areas of new ice and open water along the coast are relatively easily identified in satellite pictures and from detailed ice charts and should therefore be practical to use for model verification purposes.

5. Conclusions

ADCP observations at Falkensgrund during the ice season 2004 showed that:

Pressure ridges, defined as ice thicker than 1 m, occupied 10% of the ice cover in February, 40% in March and 22% in April, and the estimated ridged ice contribution to the total volume was 30–60%.

The ice speed was small ($<10\,\mathrm{cm\,s^{-1}}$) for most of the time (70%) and stationary ($<0.5\,\mathrm{cm\,s^{-1}}$) for only 3% of the time. High speeds (20–50 $\mathrm{cm\,s^{-1}}$) occurred in relatively well defined events. These events make up a major part (70%) of the total drift distance.

The wind/ice speed ratio was about 3% for the initial thin ice cover in early February, and the ratio was significantly lower (1–2%) during the rest of the season.

There is a general tendency that the ice is more mobile in events characterized by a large shift in wind direction.

A rough estimate, based on wind fetch and motion data, gives a compressive ice strength of $9 \times 10^4\,\mathrm{N\,m^{-2}}$, which is more than three times larger than the $2.5 \times 10^4\,\mathrm{N\,m^{-2}}$ regularly used in dynamic ice models.

6. Acknowledgments

We thank Dr. Bength Liljebladh for technical support regarding instrument configuration and data processing. This is contribution no 7 from, the centre for Earth System Science at Göteborg University (Tellus). The Swedish Meteorological and Hydrological Institute (SMHI) kindly supplied atmospheric and sea level data. Financial support was provided by Umeå Marine Science Centre (UMF) and the Swedish Research Council (VR).

References

Belliveau, D. J., Bugden, G. L., Eid, B. M. and Calnan, C. J. 1990. Sea ice velocity-measurements by upward-looking doppler current profilers. *J. Atmos. Oceanic Technol.* **7**(4), 596–602.

Granskog, M., Kartokallio, H., Kuosa, H, Thomas, D. N. and Vainio, J. 2006. Sea ice in the Baltic Sea—a review. *Estuarine, Coast. Shelf Sci.* **70**, 145–160.

Haapala, J. and Leppäranta, M. 1996. Simulating the Baltic Sea ice season with a coupled ice-ocean model. *Tellus, Ser. A* **48A**, 622–643.

IRIS, 2003. Ice Ridging Information for Decision Making in Shipping Operations. EU project homepage: http://www.tkk.fi/Units/Ship/Research/Iris/Public/

Joffre, S. M., 1982. Momentum and heat transfers in the surface layer over a frozen sea. *Boundary-Layer Met.* **24**(2), 211–229.

Jacob, D. and Omstedt, A. (eds.) 2005. BALTEX PHASE 1: 1993-2002, State of the Art Report. *BALTEX Publication* **No. 31**, 181 pages.

Leppäranta, M. 1981. On the structure and mechanics of pack ice in the Bothnian Bay. *Finnish Mar. Res.* **248**, 3–86.

Leppäranta, M. and Omstedt, A. 1990. Dynamic coupling of sea ice and water for an ice field with free boundaries. *Tellus, Ser. A* **42A**, 482–495.

Leppäranta, M. and Hakala, R. 1992. The structure and strength of first-year ice ridges in the Baltic Sea. *Cold Regions Sci. Technol.* **20**, 295–311.

Leppäranta, M. 1998. The dynamics of sea ice. Lecture notes from a summer school in Savonlinna, Finland 6–17 june 1994. In: *Physics of Ice-Covered Seas*, (ed. Matti Leppäranta). Helsinki University Press, Helsinki, 305–342.

Leppäranta, M., Sun, Y. and Haapala, J. 1998. Comparison of sea ice velocity fields from ERS-1 SAR and dynamic model. *J. Glaciol.* **44**, 248–262.

Leppäranta, M. and Omstedt, A. 1999. A review of ice time series of the Baltic Sea. *Publications Instituti Geographici Universitatis Tartuensis*, **84**, 7–10.

Leppäranta, M. 2005. *The Drift of Sea Ice*. Springer, Helsinki, 266 p.

Omstedt, A., Elken, J., Lehmann, A. and Piechura, J. 2004. Knowledge of the Baltic Sea physics gained during the BALTEX and related programmes. *Prog. Oceanogr.* **63**(1–2), 1–28.

Samuelsson, M. and Stigebrandt, A. 1996. Main characteristics of the long-term sea level variability in the Baltic Sea. *Tellus* **48A**, 672–683.

Shcherbina, A. Y., Rudnick, D. L. and Talley, L. 2005. Ice-draft profiling from bottom-mounted ADCP data. *J. Atmos. Oceanic Technol.* **22**(8), 1249–1266.

Thorndike, A. S. and Colony, R. 1982. Sea ice motion in response to geostrophic wind. *J. Geophys. Res.* **87**(C8), 5845–5852.

Thorndike, A. S., Rothrock, D. A., Maykut, G. A. and Colony, R. 1975. The thickness distribution of sea ice. *J. Geophys. Res.* **80**(33), 4501–4519.

Uotila, J. 2001. Observed and modelled sea-ice drift response to wind forcing in the northern Baltic Sea. *Tellus* **53A**, 112–128.

Zhang, Z. H. and Leppäranta, M. 1995. Modeling the influence of ice on sea level variations in the Baltic Sea. *Geophysica* **31**(2), 31–45.